Weather and Climate Extremes 40 (2023) 100564

Contents lists available at ScienceDirect

Weather and Climate Extremes

journal homepage: www.elsevier.com/locate/wace

The sources of extreme precipitation predictability; the case of the 'Wet' Red Sea Trough

Assaf Hochman [a,*], Tair Plotnik [a], Francesco Marra [b,c], Elizabeth-Ruth Shehter [d], Shira Raveh-Rubin [d], Leehi Magaritz-Ronen [d]

[a] Fredy and Nadine Hermann Institute of Earth Sciences, The Hebrew University of Jerusalem, Jerusalem, Israel
[b] Department of Geosciences, University of Padova, Italy
[c] Institute of Atmospheric Sciences and Climate, National Research Council of Italy (CNR-ISAC), Bologna, Italy
[d] Department of Earth and Planetary Sciences, Weizmann Institute of Science, Rehovot, Israel

ARTICLE INFO

Keywords:
Middle East
Dynamical systems
Chaos
Eastern Mediterranean
Numerical weather prediction
Extreme weather
Heavy precipitation

ABSTRACT

Extreme precipitation events inflict detrimental socio-economic impacts in the Eastern Mediterranean. These are mainly associated with Mediterranean cyclones or the 'Wet' Red Sea Trough (WRST). The region's weather forecasters consider the second challenging to forecast, even just a few days in advance. Here, we study the dynamic and thermodynamic factors influencing the intrinsic predictability of WRST events. With this aim, we combine insights from traditional atmospheric analysis techniques, Lagrangian air-parcel backward trajectories, and dynamical systems theory. The latter describes atmospheric states via their local dimension (d) and inverse persistence (θ), which inform us of the intrinsic predictability of the atmosphere in phase space. We compare WRST events of low (upper decile of d and θ) with high (lower decile of d and θ) predictability. We argue that low-predictability events display a significantly different atmospheric pattern. Moreover, the low-predictability events show significantly higher daily precipitation rates, more extensive spatial spread, and greater precipitation variability among events than more predictable ones. On average, low predictability events are initiated by two distinct moisture sources with different water vapor content. We conclude that the dynamical systems framework may become a valuable tool to improve the forecast of extreme precipitation events associated with the WRST by providing a priori information on their intrinsic predictability. We foresee successfully implementing such a framework for other extreme weather events and regions.

1. Introduction

Extreme precipitation events are among the most hazardous natural hazards, causing harmful socio-economic and ecologic impacts in the Eastern Mediterranean (Hochman et al., 2022b). These extremes are considered difficult to predict; thus, they have been chosen as a grand challenge of the World Climate Research Program (Alexander et al., 2015).

Eastern Mediterranean extreme precipitation events are mainly connected with Mediterranean cyclones or Red Sea Troughs (Dayan et al., 2015). The Red Sea Trough is a northern branch of the Sudan monsoon low (Ashbel, 1938; El Fandy, 1948). As soon as easterly winds flow over the mountains surrounding the Red Sea, a trough develops at their lee side (Krichak et al., 1997). The Red Sea Trough often prompts dry and warm atmospheric conditions due to the easterly to southeasterly flow from arid land regions at the surface (Tsvieli and Zangvil, 2005). However, when the surface trough axis extends toward the Mediterranean and is reinforced by an upper-level trough, it may prompt extreme precipitation and thunderstorms. Such situations are regularly termed 'Wet' Red Sea Trough (WRST; Hochman et al., 2021b; Tsvieli and Zangvil, 2005; Ziv et al., 2022b) and often result in flash floods, mainly in the south southeastern parts of the region (Fig. 1; Tsvieli and Zangvil, 2005; De Vries et al., 2013; Krichak et al., 2012; Berkovic et al., 2021). Notably, weather forecasters in the region find these events very challenging to predict (Hochman et al., 2019). In particular, numerical weather prediction model forecasts of case studies show over and underestimations related to the accurate representation of topography and moisture sources in the model (Athar and Sara, 2014; Al-Mutairi et al., 2019).

The WRST has been generally given less attention compared to

* Corresponding author.
E-mail address: Assaf.Hochman@mail.huji.ac.il (A. Hochman).

https://doi.org/10.1016/j.wace.2023.100564
Received 28 December 2022; Received in revised form 15 April 2023; Accepted 19 April 2023
Available online 20 April 2023

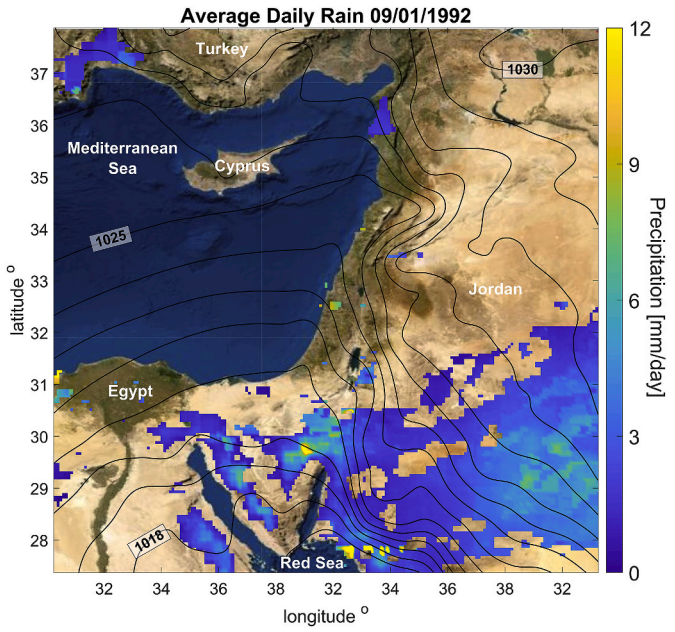

Fig. 1. Example of a WRST extreme precipitation event with high intrinsic predictability (low d & θ). Precipitation (mm d^{-1}) over Israel for January 9th 1992, in color shading. The black contours represent mean sea level pressure (hPa). (For interpretation of the references to color in this figure legend, the reader is referred to the Web version of this article.)

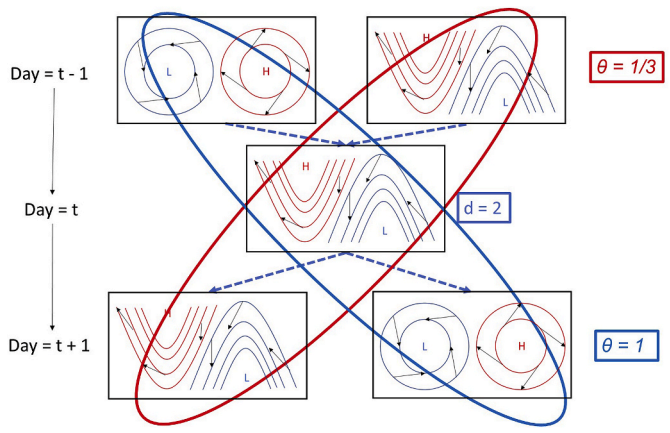

Fig. 2. An intuitive schematic of d and θ computed for tentative atmospheric states. The local dimension (d) is related to the number of possible patterns preceding and following the state being analyzed at day t (here, $d = 2$), and θ is the inverse of the persistence. When the Red Sea Trough persists for three days (red ellipse), then $\theta = 1/3$. If the synoptic configuration changes every time step (blue path), then $\theta = 1$. Inspired by a figure from Hochman et al. (2022a) and Rodrigues et al. (2018). (For interpretation of the references to color in this figure legend, the reader is referred to the Web version of this article.)

Mediterranean cyclones. Nevertheless, studies have concentrated on identifying and characterizing it in gridded climate data (Ziv et al., 2022b; Tsvieli and Zangvil, 2005; Saaroni et al., 2019; Krichak et al., 2012; Alpert et al., 2004; Awad and Almazroui, 2016). However, recent attempts to extract an atmospheric proxy identifying a WRST and its precipitation intensity did not yield significant separation between dry and wet Red Sea Trough events (Ziv et al., 2022b). Here, we identify a Red Sea Trough according to the semi-objective synoptic classification (Alpert et al., 2004). The classification has been recently upgraded to include upper-level variables (Ludwig and Hochman, 2022). This categorization has been proven useful in reflecting the subtle characteristics of Eastern Mediterranean weather types, including the Red Sea Trough (Hochman et al., 2018; Hochman et al., 2021b). We classify the 'Wet' configuration of the Red Sea Trough by leveraging data from the Climate Hazards Group Infrared Precipitation with Stations dataset over the Eastern Mediterranean domain (CHIRPS version 2; Fig. 1; Funk et al., 2015).

The ability to predict extreme weather has traditionally relied solely on numerical weather prediction models. Numerical Weather Prediction (NWP) improved incredibly in recent decades due to better data assimilation, higher resolution, and thus extended forecast horizons (Alley et al., 2019). However, implementing NWP models in a purely deterministic manner is subject to considerable limitations due to the chaotic nature of atmospheric dynamics (Lorenz, 1963). Hence, the leading modeling revolution in the last two decades is ensemble-forecasting systems that use a set of perturbed initial conditions to produce a range of probable future atmospheric states (Palmer, 2000). Nevertheless, there are still considerable limitations to NWP. Some of these limitations, particularly extensive computational costs, can be mitigated by leveraging recent progress in dynamical systems theory. These developments allow us to quantify the intrinsic predictability of atmospheric states in phase space. The intrinsic predictability is innately linked to the local dimension (d), which estimates the possible number of options the atmospheric state can evolve to and from and the inverse of the persistence time (θ; Fig. 2; Faranda et al., 2017). Indeed, a highly persistent (low θ), low-dimensional (low d) state shall be more predictable than a low-persistence (high θ), high-dimensional (high d) one (Messori et al., 2017). The dynamical systems framework has been recently implemented in a few studies focusing on atmospheric extremes (e.g., Hochman et al., 2022; Hochman et al., 2021a,b,c; Rodrigues et al., 2018; Wedler et al., 2023).

The intrinsic predictability of precipitation extremes may be strongly influenced by dynamic and thermo-dynamic factors (Dayan et al., 2015). A framework that permits a quantitative understanding of the processes leading to precipitation extremes is based on tracking the air parcel characteristics and source. The Lagrangian viewpoint offers complementary insights into the underlying dynamics and predictability of weather extremes (Hochman et al., 2021c). Air-mass trajectories can indicate the source region and any coherent evolution of the thermo-dynamical characteristics of the air parcels during the time prior to precipitation (Sodemann et al., 2008). In the Eastern Mediterranean, air-mass trajectories have served to locate the moisture source of precipitation and identify cyclone-related air streams in multiple case studies of heavy precipitation and strong winds (Raveh-Rubin and Wernli, 2016). In addition, backward trajectories were used to quantify the relative contribution of diabatic and adiabatic processes for warm and dry extremes (Berkovic and Raveh-Rubin, 2022). A recent systematic investigation of the air parcels arriving in Israel during WRSTs revealed that even in the events considered to have tropical characteristics, most air masses did not arrive from tropical latitudes (Ziv et al., 2022b).

This study aims to identify the main factors influencing the intrinsic predictability of extreme precipitation events associated with the WRST using the abovementioned approaches. We organize the manuscript as follows: Section 2 lays out the methodology used, including the data (Sect. 2.1), classification of extreme precipitation events (Sect. 2.2), dynamical systems analysis (Sect. 2.3), and air parcel trajectories (Sect. 2.4). The results section provides insight into the time series dynamics of extreme precipitation events, and how it is related to the atmospheric configuration (Sect. 3.1), and then it presents traditional atmospheric analysis (Sect. 3.2) and a Lagrangian view of low vs. high predictability events selected case studies (Sect. 3.3). Finally, Section 4 offers summary and concluding remarks.

2. Data and methods

2.1. Data

We based the Red Sea Trough classification, the air-parcel backward tracking, and the dynamical systems analysis on the fifth generation of the European Center for Medium-Range Weather Forecasting Reanalysis data (ERA5; Hersbach et al., 2020). We bilinear interpolated the atmospheric fields to a 0.5° × 0.5° horizontal grid spacing. We used daily (precipitation extremes classification and dynamical systems analysis) and 3-hourly (air-parcel backward tracking) temporal resolutions from 1979 to 2019.

Due to their grid spacing, reanalysis products cannot explicitly resolve convective precipitation processes. Alternative sources are thus recommended for the case of extreme precipitation (Alexander et al., 2020). We used precipitation estimates from the Climate Hazards Group InfraRed Precipitation with Station version 2 (CHIRPS; Funk et al., 2015). CHIRPS is created using infrared precipitation estimates from geostationary satellites merged with a rain gauge climatology procedure. It includes global land-only daily precipitation estimates at 0.05° × 0.05° horizontal grid spacing from 1981 to 2019. Although the product is aggregated to daily scales, the high spatial and temporal resolutions of the infrared sensors onboard geostationary satellites (Kidd and Levizzani, 2011) allow capturing the short-living and localized convective systems typical of the WRST (Hochman et al., 2022; Armon et al., 2019). CHIRPS is considered robust and is primarily used in climatological studies over regions with comparable precipitation climatology and characteristics as the Eastern Mediterranean (Dinku et al., 2018; Satgé et al., 2020; Marra et al., 2022).

2.2. Classification of extreme precipitation events associated with the WRST

First, we classified the daily weather types over the Eastern Mediterranean (Fig. 1; 30–40°E, 27.5–37.5°N) using the upgraded semi-objective synoptic classification algorithm (Alpert et al., 2004; Ludwig and Hochman, 2022). Specifically, the classification uses the days in 1985 and the winter of 1991–1992, classified into the regional weather types by expert forecasters, as 'ground truth' (426 days). Then, it finds the minimum Euclidean distance between a day of interest and the ground truth. The day with the minimum distance is labeled a specific weather type. This classification represents the regional weather conditions well (Hochman et al., 2018) and is based on daily mean surface air temperature at 2-m (T2m), Sea-Level-Pressure (SLP), and 500 hPa geopotential height (Z500) fields from the ERA5 reanalysis. We selected only those days that are categorized as a Red Sea Trough.

In detail, the original classification used only surface variables, including U, V, T, and Z at 1000 hPa (Alpert et al., 2004). Ludwig and Hochman (2022) used the same classification procedure. Still, instead of the abovementioned variables, the authors used T2m, SLP, and Z500, which are also the variables we computed the dynamical systems metrics on (see Sect. 2.3). Moreover, the abovementioned variables include sea-land contrast (T2m), synoptic (SLP), and large-scale (Z500) features. We evaluated our classification (Ludwig and Hochman, 2022) ability to identify the Red Sea Trough. To do so, we randomly selected 100 days classified as a Red Sea Trough. Then, we tested if these days were really a Red Sea Trough by inspecting the synoptic maps of these 100 days according to the evaluation suggested by Saaroni et al. (2019). We find that using T2m, SLP, and Z500 in the classification procedure improves the identification of a Red Sea Trough from 62% in the original classification (62 real Red Sea Trough days out of 100) to 87% in our classification. We further note that transitioning from NCEP/NCAR reanalysis, used in the original classification and Ziv et al. (2022a, b), to ERA5 reanalysis but with the original variables (U, V, T, and Z at 1000 hPa) improved the identification of a Red Sea Trough from 62% to 72%.

The classification of precipitation events into extreme and light events was based on the CHIRPS data set. It focuses on land areas within the region used to classify the Red Sea Trough days (Fig. 1). We removed a few grid points in the Saudi desert due to apparent noise in the CHIRPS estimates. In total, we used ~27500 grid points. We then defined WRST events at the regional scale as ≥ 1 consecutive days classified as a Red Sea Trough, in which at least one grid point is wet, i.e., precipitation $\geq$ 0.1 mm. At each grid point, we retained the maximum daily precipitation during each event (in case the event lasts more than one day) to obtain a list of WRST daily maxima. Those events with at least 15 grid points above the local 98th percentile of the WRST events were defined as extreme precipitation events. Similarly, we defined events with less than 100 grid points exceeding the local 30th percentile of the WRST events as light precipitation events. Thus, we retained 289 (269) extreme (light) precipitation events, which are each ~20% of all WRST events. We chose these quantile thresholds to divide the dataset into equally populated extreme and light events groups. We note here that the rainfall study area is based on the synoptic classification domain (Fig. 1). Nevertheless, before starting our analyses, we tested three additional possible domains: Israel, arid ($<$400 mm y^{-1}), and non-arid climates ($>$400 mm y^{-1}). The results presented in this study are rather insensitive to the domain used. This is a non-trivial finding. The reason for this may relate to our focus on extreme precipitation events with a minimum spatial extent and structure. Practically, we seek the strongest events that impact large areas.

2.3. Dynamical systems metrics for estimating the intrinsic predictability

To characterize the intrinsic predictability of WRST events, we depend on a method that merges Poincaré recurrences with extreme value theory (Lucarini et al., 2012; Lucarini et al., 2016). This point of view permits the computation of instantaneous properties of chaotic dynamical systems. It is, therefore, very well suited for studying the atmosphere's time series dynamics (Faranda et al., 2017). We took the time series of two-dimensional atmospheric maps as a long trajectory in phase space. We focused on two metrics. The local dimension (d) is a proxy for the number of active degrees of freedom the trajectory can discover locally. The inverse of persistence (θ) is linked to the more traditional notion of persistence (Hochman et al., 2019). Both metrics are strongly related to the intrinsic predictability of the atmosphere's evolution, such that a high d and θ correspond to a low intrinsically predictable atmospheric state and vice versa (Messori et al., 2017). We computed the inverse of the persistence time of an atmospheric state of interest using the extremal index estimator (Süveges, 2007). The computation of d and θ comes from the understanding that the cumulative probability distribution of the system recurrences converges to the Generalized Pareto Distribution exponential member that is applicable for modeling the tails of physical distributions (Faranda et al., 2017). We point the reader to additional details regarding the derivation of the metrics (Faranda et al., 2019; Hochman et al., 2022), and Fig. 2 for an intuitive schematic describing the dynamical systems metrics.

Previous studies have shown that d and θ exhibit a seasonal cycle (Faranda et al., 2017; Rodrigues et al., 2018; Hochman et al., 2022c). Therefore, we removed the seasonal cycle before comparing different WRST events. We must deseasonalize the metrics to study the anomalies as we compare different events during different parts of the year. Note that the selected events do not have a preference for a specific time of year. We estimated the seasonal cycle by averaging the metrics over all years for a specific time step, repeating this for all time steps within a year, and eventually smoothing the series via a 30-day moving average (Hochman, 2021a,c,2022c; Hochman et al., 2022).

The dynamical systems framework has been applied to various atmospheric datasets (e.g., De Luca et al., 2020; Pons et al., 2020; Brunetti et al., 2019). Here, we computed d and θ for daily SLP, Z500, and T2m fields from the ERA5 reanalysis over the Eastern Mediterranean (Fig. 1), consistent with the variables used for the synoptic classification (see Sect. 2.2). We defined low and high intrinsically predictable days as the

upper and lower deciles of d and θ anomalies, respectively. We chose this threshold as a compromise between keeping the extreme events and gathering a sizeable number of cases for robustness.

We produced mean composite maps to understand the differences between subgroups of WRST events and their predictability. We tested for significant differences at the 5% level using a two-sided student's T-test (for SLP, Z500, T2m, and T850 maps) and a bootstrap sampling test with 10^4 realizations (for precipitation).

2.4. Air-parcel trajectories

We computed 5-day backward air-parcel trajectories using the Lagrangian analysis tool (LAGRANTO 2.0; Sprenger and Wernli, 2015; Wernli and Davies, 1997). LAGRANTO uses the entire 3-D wind field from ERA5 to calculate the air-mass trajectory. Trajectories are initialized at 00 UTC from fixed points in the analysis domain (Fig. 1; 30–40°E, 27.5–37.5°N) every 50 hPa between 950 and 800 hPa on the first day of the event. We filtered the classified WRST events trajectories to use the ones originating from grid points with more than 0.5 mm of precipitation. We obtained insights into the characteristics of the air parcels by tracking the specific humidity along the trajectories. Changes in the specific humidity indicate moisture uptake due to turbulent fluxes, evaporative processes, or convection in or above the boundary layer (Sodemann et al., 2008).

3. Results

3.1. Dynamics of WRST extreme vs. light precipitation events

We first analyzed the differences between extreme and light

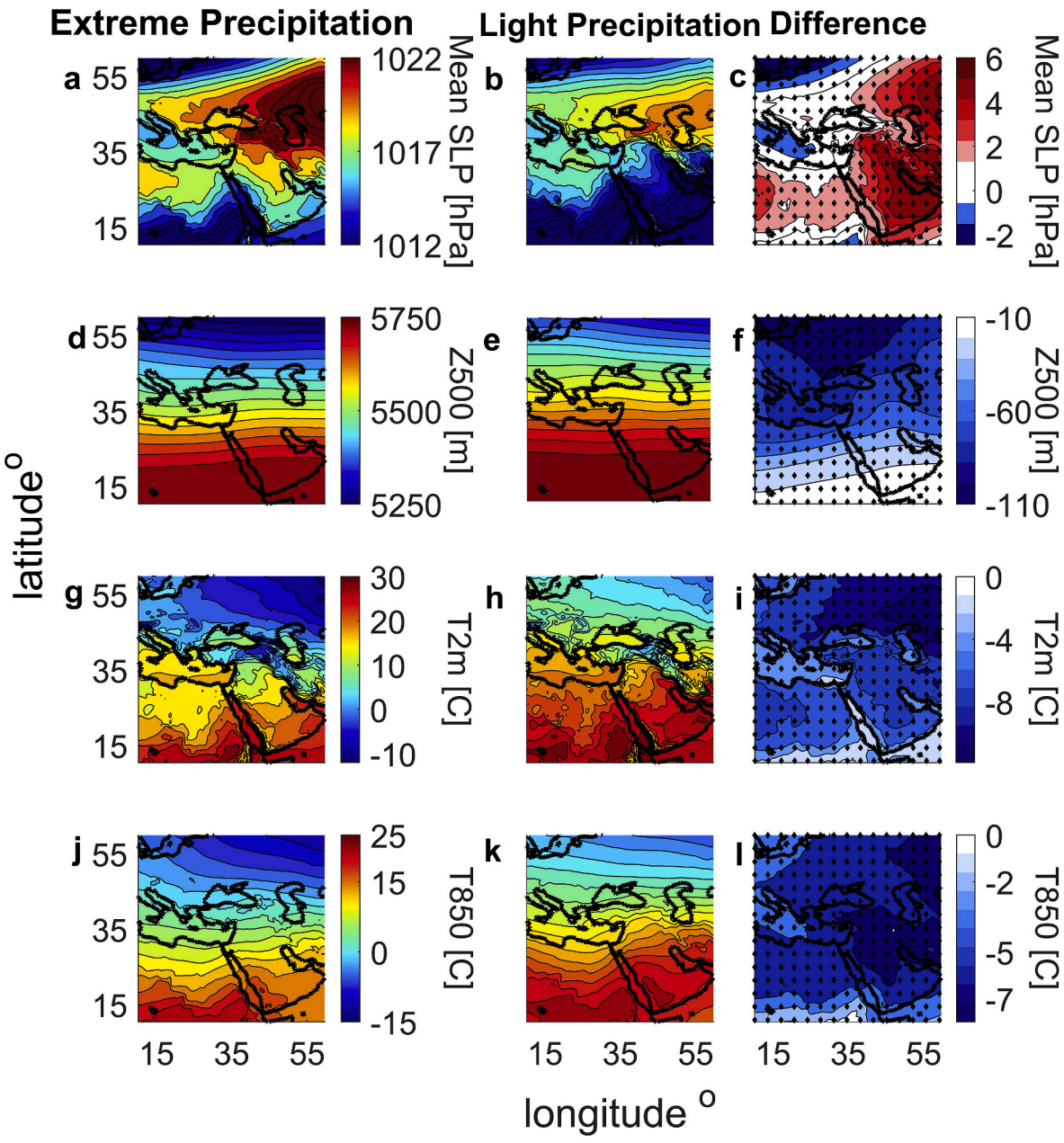

Fig. 3. Comparison between extreme (left panels – 289 events) vs. light (middle panels – 269 events) precipitation events associated with the WRST in 1979–2019. Average daily mean Sea Level Pressure (SLP in hPa; a-c), 500 hPa geopotential height (Z500 in m; d-f), 2-m temperature (T2m in °C; g-i), and 850 hPa temperature (T850 in °C; j – l). The difference between extreme and light precipitation events is displayed (right panels). Using a two-sided student T-test, black crosses denote significant differences at the 5% level.

precipitation events (see Sect. 2.2 for the definition). From an atmospheric dynamics point of view, there are a few apparent differences between the two subgroups (Fig. 3). In the case of extreme precipitation, Western Asia is dominated by an extensive high, and the Red Sea Trough is more distinct (Fig. 3 a-c). The Z500 patterns of extreme precipitation events display lower average geopotential heights than light precipitation events, particularly pronounced over the Eastern part of the Mediterranean Sea, enhancing the large-scale forcing of air uplift in the Eastern Mediterranean (Fig. 3 d-f). Finally, the temperatures at the surface and at the 850 hPa level in the extreme precipitation events display significantly lower temperatures than the light precipitation ones (Fig. 3 g-l).

Next, we focused on the extreme precipitation events and separated them into subgroups, i.e., upper and lower deciles of d and θ. As such, we studied the atmospheric factors influencing the anomalies of d and θ and consequently related this to the differences in the intrinsic predictability of these events. The upper and lower deciles of the d and θ metrics exhibit substantial atmospheric differences (Figs. 4 and 5, respectively). The upper decile of d events has lower SLP values, more pronounced over Cyprus and Jordan (Fig. 4 a-c). The high and low θ events exhibit similar SLP differences compared to those between the subgroups of d (Fig. 5 a-c). We, therefore, suggest that the airflow in the low predictability events is influenced by the Mediterranean Sea in addition to more southerly locations (see also Sect. 3.2). The main difference between the Z500 patterns of the high and low d subgroups is the orientation of the trough axis (Fig. 4 d-f). Indeed, the trough axis is oriented in the northeast-southwest direction in the high d events (Fig. 4 d), whereas the trough direction is northwest-southeast in the low d events (Fig. 4 e). This implies colder air transport from northerly locations in the high d events compared to the low d events on the rear side of the trough. A somewhat different picture arise from comparing high and low θ events (Fig. 5 d-f). The high θ (low persistence) events display lower Z500 values (Fig. 5 d). However, the low θ events display a pronounced trough tongue reaching the Mediterranean Sea (Fig. 5 e). Finally, the temperature at the surface displays lower gradients in the west-east direction that mainly relate to land-sea temperature difference, with lower temperatures over the Mediterranean, in both the high d and θ events (Fig. 4 g-i and 5 g-i, respectively). The differences in temperature may relate to seasonal differences; however, the individual events were found to be distributed evenly during various seasons, for both high and low d and θ subgroups.

To summarize, there are substantial differences between high and low d and θ extreme precipitation events in terms of the atmospheric flow influencing these metrics and, consequently, the intrinsic predictability of WRST events. The near-surface patterns influencing d and θ are very similar, considering the SLP and T2m variables. However, for the upper-level Z500 variable, the factors influencing d and θ are somewhat different. We note that each composite in Figs. 4 and 5 is composed of different members, as the measure of d and θ depends on the variable used for its definition. We next examined their relationships.

3.2. Dynamics of low vs. high predictability WRST extreme precipitation events

First, we selected high and low intrinsically predictable extreme precipitation events where both d and θ are at the distribution's upper (low predictability) or lower (high predictability) decile. We centered our definition on the dynamical systems metrics computed for the T2m

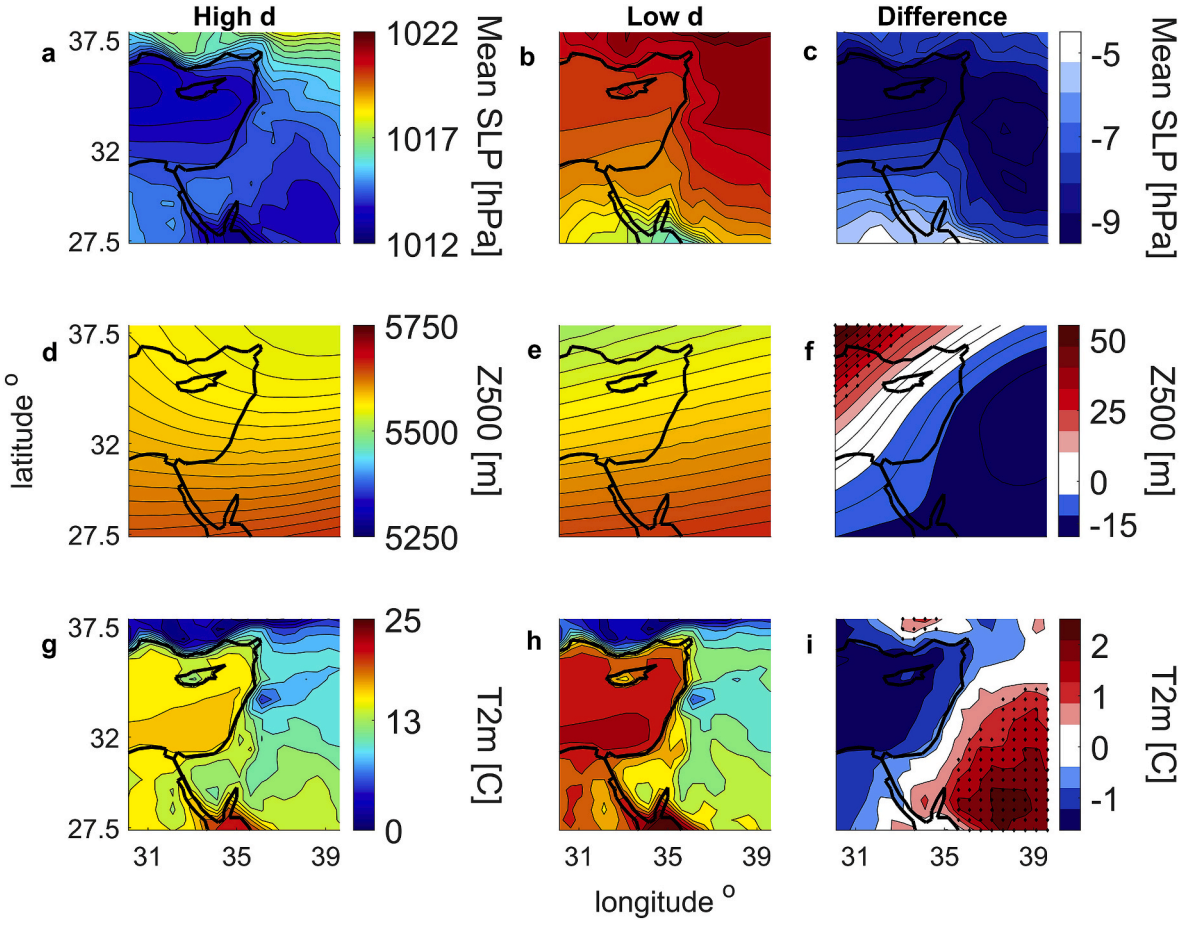

Fig. 4. Same as Fig. 3 but comparing high (left panels) vs. low (middle panels) local dimension (d) extreme precipitation events. Note that d is calculated separately for each variable; thus, the composited days do not necessarily overlap.

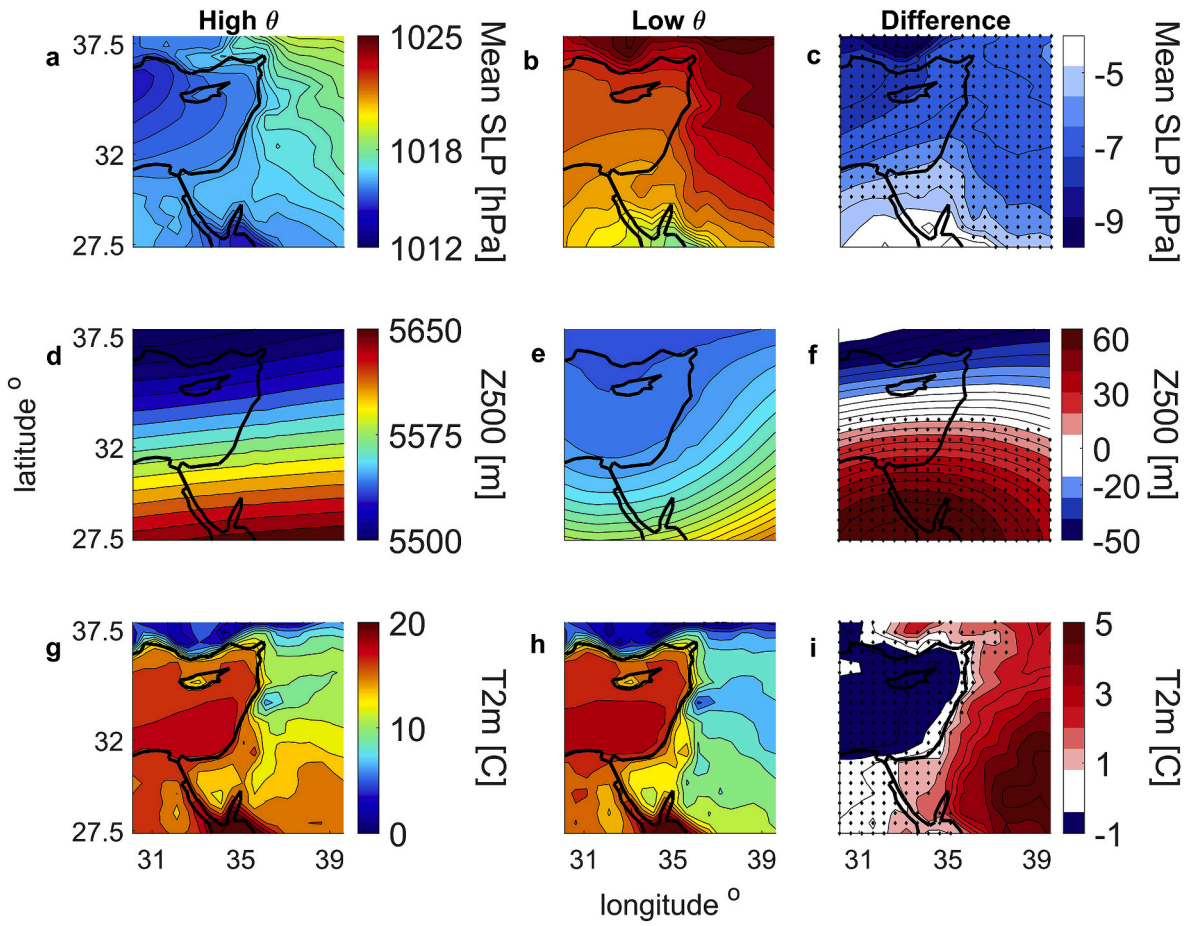

Fig. 5. Same as Fig. 3 but comparing high (left panels) vs. low (middle panels) inverse persistence (θ) of extreme precipitation events.

variable since it demonstrates a significantly higher correlation (0.63) between d and θ compared to SLP (0.23) and Z500 (0). We identified 14 low and 16 high-predictability events (Fig. 6).

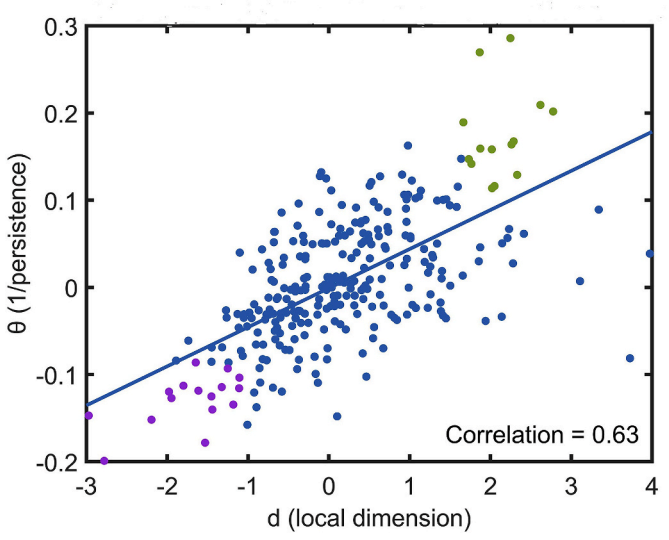

Fig. 6. Scatter plot of local dimension (d) vs. inverse persistence (θ) anomalies computed for extreme precipitation events associated with the WRST. The metrics are computed on the 2-m temperature (T2m) variable. Selected anomalous low predictability (high d & θ – 14 events) events are in green, and high predictability (low d & θ – 16 events) are in purple. Figs. 7–10 are based on the selected events. (For interpretation of the references to color in this figure legend, the reader is referred to the Web version of this article.)

Next, we analyzed the differences between the abovementioned low and high-predictability events (Fig. 7). Low predictability events are accompanied by an additional low-pressure minimum over the Eastern Mediterranean and the SLP minimum over the Red Sea, which is deeper as well, compared to the overall higher pressure to the north of high-predictability events. The temperature at the surface and 850 hPa exhibits lower temperature gradients in the west-east direction, with higher temperatures over the Mediterranean Sea in the low-predictability events (Fig. 7 g-l). Finally, the upper-level trough at Z500 in the low-predictability events is more profound, and the airflow is southwesterly compared to northwesterly in the high-predictability events (Fig. 7 d-f).

Fig. 8 displays the differences between low and high-predictability extreme precipitation events in their maximum daily precipitation patterns. Indeed, the low-predictability events exhibit higher daily precipitation values and more extensive spatial extension (Fig. 8 a-c). Yet, southern and eastern parts of the domain exhibit lower precipitation rates in low predictability events. However, an area comparison can be misleading when comparing events typified by highly localized, convective precipitation. In addition, the standard deviation in maximum precipitation between the events is larger in the low-predictability events (Fig. 8 d-f). These findings advise that the dynamical systems metrics are linked with the maximum surface precipitation and its spatial patterns, which may prompt using these metrics to improve the predictability of extreme precipitation events.

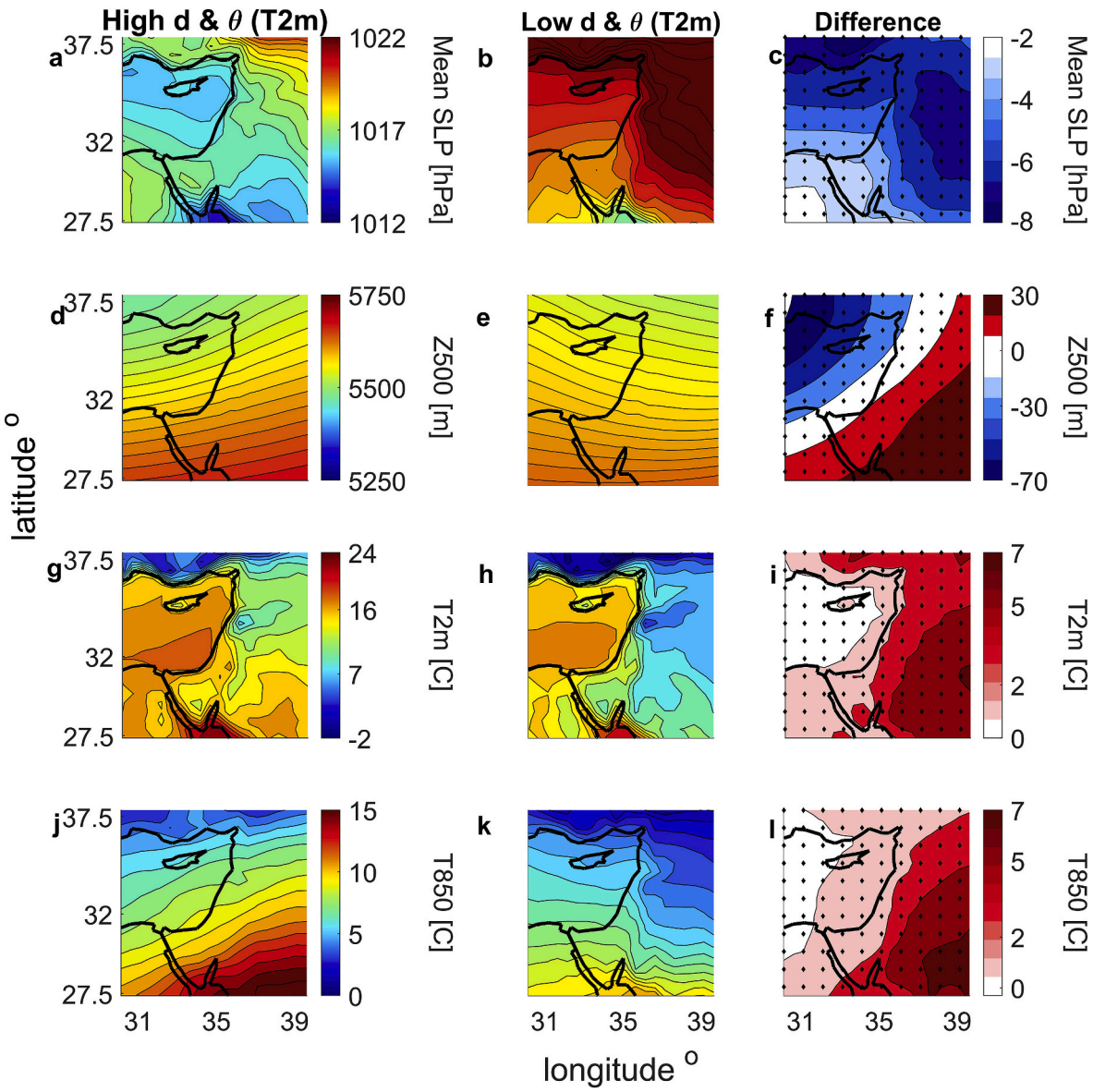

Fig. 7. Same as Fig. 3 but comparing high (left panels) vs. low (middle panels) predictability of extreme precipitation events associated with the WRST. We define the low and high predictability events in Fig. 6.

3.3. Air-parcel history of low vs. high predictability WRST extreme precipitation events

The backward trajectories of air parcels preceding low vs. high predictability events display considerable differences (Figs. 9 and 10). The analysis illustrates that, on average, the flow preceding a high-predictability event has a roughly zonal orientation. Indeed, most air parcels originate from relatively localized regions in the Eastern part of the Mediterranean Sea (Fig. 9 a, c; in purple). The air parcels in the low-predictability events originate from more distant areas both in meridional and zonal directions (Fig. 9 a, c; in green). The initial pressure level of the air parcels shows a slight widening of the distribution in the low-predictability events, indicating that more air parcels in these cases originate closer to the surface compared to the mid-troposphere in the more predictable events (Fig. 9 b).

An implication of the parcel height distribution shift to lower tropospheric levels is the moisture content of the air parcels reaching the Eastern Mediterranean. Examination of the humidity evolution leading to low vs. high predictability events shows that at $\geq$ 96 h prior to the event, there are relatively small differences between the distribution of specific humidity content of the air masses, with higher values for the low-predictability events (Fig. 10 a). However, closer to the event's time, only the low predictability humidity distribution evolves to a bimodal distribution, with two peaks in the high (~5 g/kg) and the lower (~1 g/kg) specific humidity compared to high-predictability events (Fig. 10 b, c). The interaction between air parcels of such different properties could lead to rapid precipitation development and, thus, a decrease in the overall predictability of the event. This process is particularly evident in the last 48 h before the event (Fig. 10 c), suggesting that the low predictability of such events results from short-term contributions before the onset of precipitation. A merging of relatively high with low humidity air parcels, as suggested by the greater meridional extent of the air-mass origins of low-predictability events, is proposed here as a unique factor degrading the predictability of WRST extreme precipitation events.

4. Summary and conclusions

Predicting extreme precipitation events is critical for increasing preparedness and thus reducing their potential impact. This is

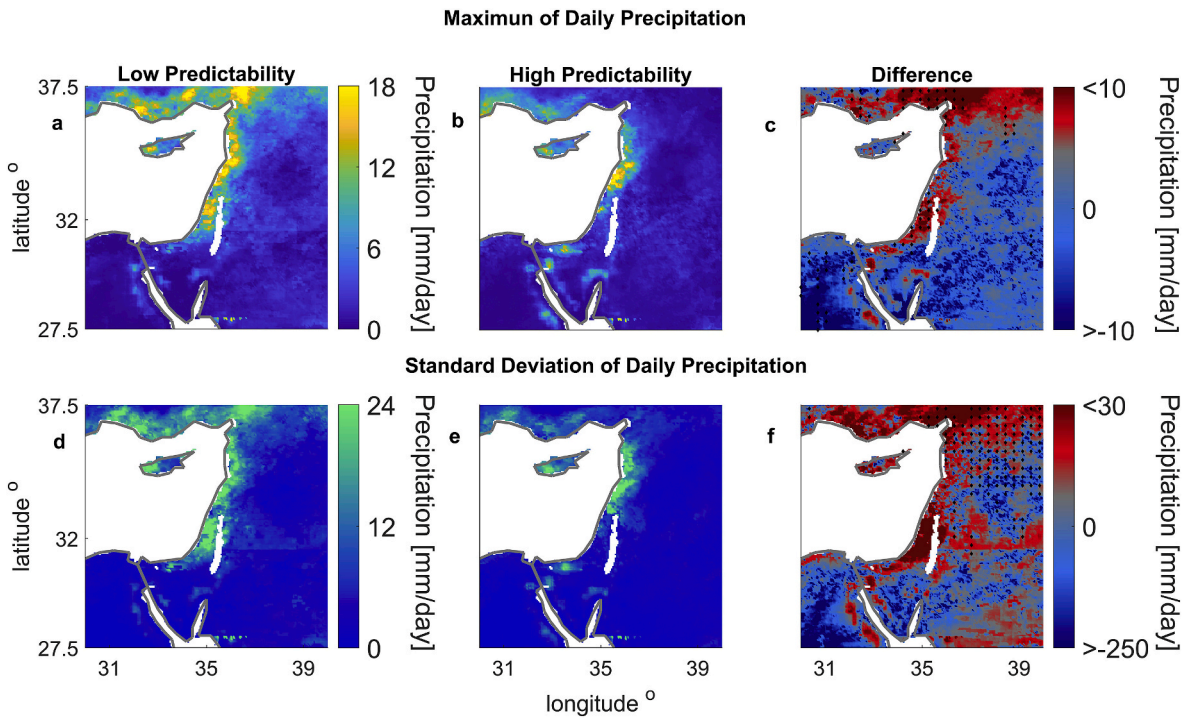

Fig. 8. Mean composite maps of maximum (a–c) and standard deviation (d–f) of daily precipitation over the Eastern Mediterranean. (a, d) Low predictability events, (b, e) high predictability events, and (c, f) difference between low and high predictability events. We define the low and high predictability events in Fig. 6. Black crosses denote significant differences at the 5% level using a bootstrap test with 10^4 realizations.

particularly challenging in an epoch of fast climate change, as the frequency of the synoptic conditions characterizing extreme weather in a region may change dramatically (Hochman et al., 2022b; David-Novak et al., 2004; Hochman et al., 2018). While the community has given most of the attention to Mediterranean cyclones, the WRST also has the potential for extensive damage. It may bring torrential rains, thunderstorms, debris flows, and flooding (De Vries et al., 2013) and is considered difficult to forecast accurately (Gasch et al., 2017). Despite this, the predictability of WRST has received less consideration in the literature so far.

Here, we combine dynamical systems theory, traditional atmospheric analysis techniques, and Lagrangian backward air parcel trajectories to identify the main factors influencing the intrinsic predictability of such events. We define extreme precipitation events associated with the WRST using an upgraded synoptic classification algorithm (Alpert et al., 2004; Ludwig and Hochman, 2022) using ERA5 reanalysis variables with high-resolution daily precipitation data from the CHIRPS version 2 data set.

Our main findings are as follows:

i. Extreme precipitation events associated with the WRST display significant atmospheric pattern differences compared to light precipitation events associated with the same system.
ii. *Low-predictability events display a different atmospheric pattern compared to high-predictability ones.* Low-predictability events are associated with lower SLP values over Cyprus and Jordan (Ziv et al., 2022a), and a different orientation/depth of the upper-level trough. Indeed, the low predictability of extreme precipitation events in the Western Mediterranean is also linked with the location and intensity of the cut-off low (Khodayar et al., 2022).
iii. *We provide evidence that the dynamical systems metrics relate to maximum precipitation amounts, spatial spread, and precipitation variability.* These metrics may become a helpful tool to improve our ability to forecast extreme precipitation events associated with the WRST.
iv. The *backward air-parcel trajectory analysis provides novel insights into the origin and moisture evolution that prompt low-predictability events.* We argue that low-predictability events are generated when air parcels with very different moisture contents, particularly in the last 48 h before the event time, converge over the region. This relatively short period before the event was also found to be critical when forecasting the region's cold spells (Hochman et al., 2022c).

As a caveat, we note that the dynamical systems framework still holds some interpretation challenges. For example, deciding on the atmospheric variable or vertical level that best characterizes a weather event's intrinsic predictability is not always straightforward. Moreover, the quantitative results we present may depend on the choice of threshold to define extreme/light precipitation and low/high predictability events. Finally, the Red Sea Trough has recently received attention regarding how it is classified in reanalysis data (Ziv et al., 2022b). We note that our framework of analyzing intrinsic predictability could be useful when analyzing other types of classification procedures in the future.

We envisage that the innovative perspective and framework offered here, which leverages dynamical systems and atmospheric dynamics points of view for identifying the primary sources of extreme weather predictability, outlines a research direction with great potential. At the same time, care must be taken in interpretation. We trust, however, that it can be applied to other regions and weather extremes.

Author contributions

Conceptualization: AH, FM, LMR, SRR, Data curation: AH, FM, LMR, TP, ERS, Formal analysis: AH, FM, LMR, TP, ERS, Funding acquisition: AH, SRR, Investigation: AH, FM, LMR, ERS, SRR, Methodology: AH, FM, LMR, SRR, Project administration: AH, SRR, Supervision: AH, SRR, LMR,

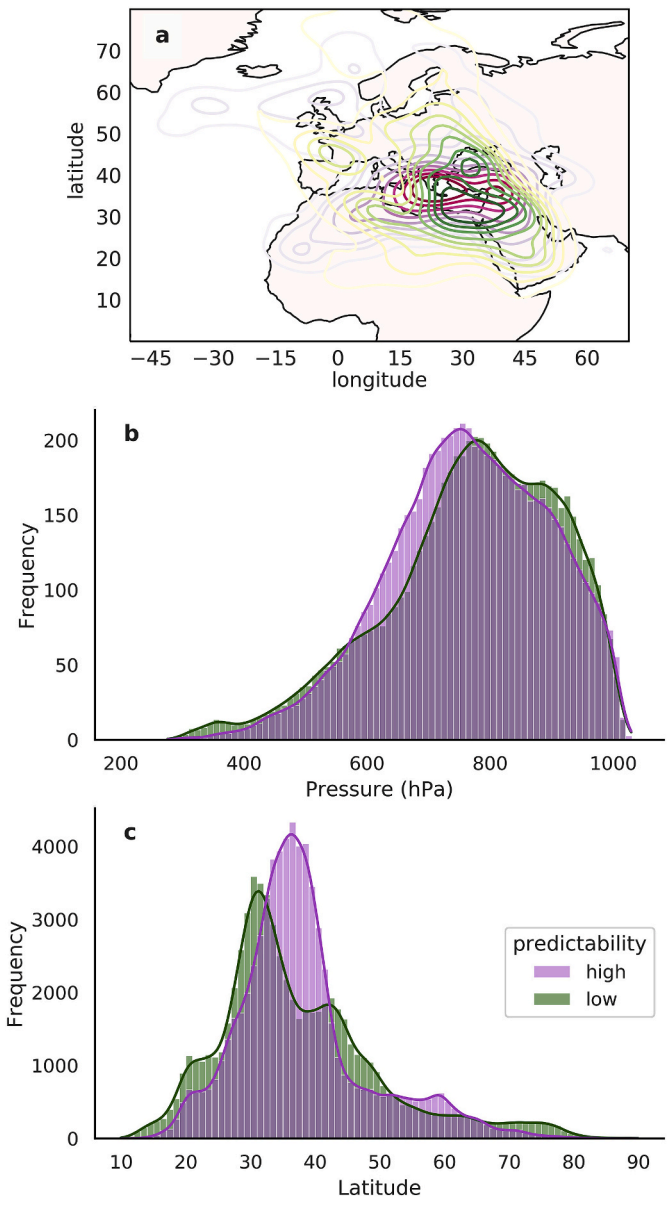

Fig. 9. (a) A spatial density plot (Kernel Density Estimation; KDE) of the trajectories at 96 h prior to arrival for low (green) and high (purple) predictability extreme precipitation WRST events. (b) Histograms of pressure level (hPa) for low (green) and high (purple) predictability of extreme precipitation WRST events. (c) Same as (b) but for latitude (°N). We define the low and high predictability events in Fig. 6. Zero hours corresponds to the first day of an event at 00 UTC. (For interpretation of the references to color in this figure legend, the reader is referred to the Web version of this article.)

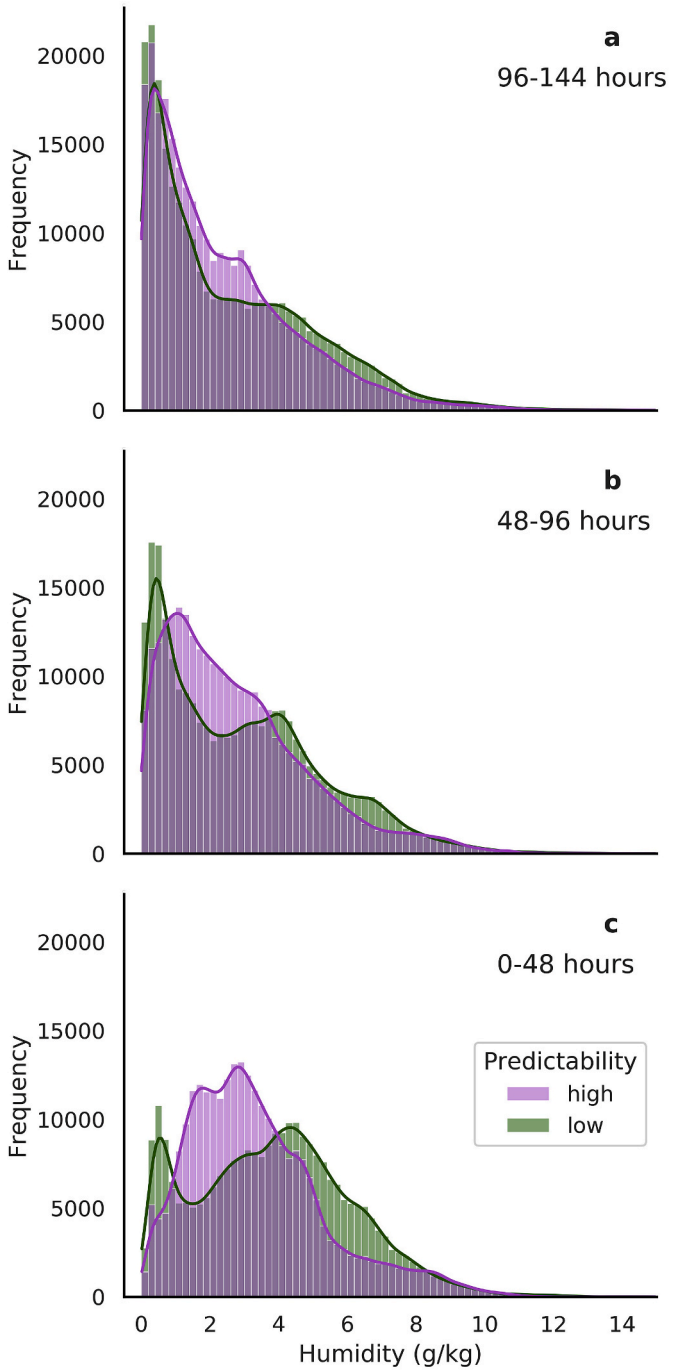

Fig. 10. Histograms of specific humidity (g/kg) for high vs. low predictability extreme precipitation WRST events at (a) 96–144 h, (b) 48–96 h, and (c) 0–48 h before the events. We define the low and high predictability events in Fig. 6. Zero hours corresponds to the first day of an event at 00 UTC.

Visualization: AH, LMR, TP, Writing - original draft: AH, Writing - review & editing: AH, FM, LMR, TP, SRR.

Data statement

We based the analysis in this study on the European Centre for Medium-Range Weather Forecast ERA5 reanalysis (Hersbach et al., 2020) and the CHIRPS data set (Funk et al., 2015). The synoptic classification is available through (Alpert et al., 2004; Ludwig and Hochman, 2022). The dynamical systems analysis code is freely available at https://ch.mathworks.com/matlabcentral/fileexchange/95768-attractor-local-dimension-and-local-persistence-computation. The backward computing of trajectories code is freely obtainable at https://iacweb.ethz.ch/staff/sprenger/lagranto/.

Funding

The Pazi Foundation (grant #434) and the Ministry of Science, Innovation, and Technology of Israel (grant #4749) partly fund the contribution of AH and TP. CARIPARO Foundation partially supported FM through the Excellence Grant 2021 to the "Resilience" project. The de Botton Center for Marine Sciences at the Weizmann Institute of Science partially supported the contribution of LMR.

Declaration of competing interest

The authors declare that they have no known competing financial interests or personal relationships that could have appeared to influence the work reported in this paper.

Data availability

Data will be made available on request.

Acknowledgments

AH thanks the Hebrew University of Jerusalem for technical support and for funding of article processing charges and open access of this article.

References

Alexander, L., et al., 2020. Intercomparison of annual precipitation indices and extremes over global land areas from in situ, space-based and reanalysis products. Environ. Res. Lett. 15 (5), 055002.
Alexander, L., et al., 2015. The World climate research Program grand challenge on extremes – WCRP-ICTP summer school on attribution and prediction of extreme events. Weather Clim. Extrem. 9, 1–78.
Alley, R., Emanuel, K., Zhang, F., 2019. Advances in weather prediction. Science 363 (6425), 342–344.
Al-Mutairi, M., Basset, H., Morsy, M., Abdeldym, A., 2019. On the effect of Red Sea and topography on rainfall over Saudi arabia: case study. Atmosphere 10 (11), 669.
Alpert, P., Osetinski, I., Ziv, B., Shafir, H., 2004. Semi-objective classification for daily synoptic systems: application to the Eastern Mediterranean climate change. Int. J. Climatol. 24, 1001–1011.
Armon, M., Morin, E., Enzel, Y., 2019. Overview of modern atmospheric patterns controlling rainfall and floods into the Dead Sea: implications for the lake's sedimentology and paleohydrology. Quat. Sci. Rev. 216, 58–73.
Ashbel, D., 1938. Great floods in Sinai Peninsula, Palestine, Syria and the Syrian Desert, and the influence of the red sea on their formation. Q. J. R. Meteorol. Soc. 64, 635–639.
Athar, H., Sara, A., 2014. Surface temperature forecast skill comparison for the west coast of Saudi Arabia. Atmósfera 27 (3), 287–303.
Awad, A., Almazroui, M., 2016. Climatology of the winter Red Sea Trough. Atmos. Res. 182, 20–29.
Berkovic, S., Mendelsohn, O., Ilotoviz, E., Raveh-Rubin, S., 2021. Self-organizing map classification of the boundary layer profile: a refinement of Eastern Mediterranean winter synoptic regimes. Int. J. Climatol. 41, 3317–3338.
Berkovic, S., Raveh-Rubin, S., 2022. Persistent warm and dry extremes over the eastern Mediterranean during winter: the role of North Atlantic blocking and central Mediterranean cyclones. Q. J. R. Meteorol. Soc. 148 (746), 2384–2409.
Brunetti, M., Kasparian, J., Vérard, C., 2019. Co-existing climate attractors in a coupled aqua-planet. Clim. Dynam. 53, 6293–6308.
David-Novak, H., Morin, E., Enzel, Y., 2004. Modern extreme storms and the rainfall thresholds for initiating debris flows on the hyperarid western escarpment of the Dead Sea, Israel. GSA Bulletin 116 (5–6), 718–728.
Dayan, U., Nissen, K., Ulbrich, U., 2015. Review Article: atmospheric conditions inducing extreme precipitation over the eastern and western Mediterranean. Nat. Hazards Earth Syst. Sci. 15, 2525–2544.
De Luca, P., Messori, G., Pons, F., Faranda, D., 2020. Dynamical systems theory sheds new light on compound climate extremes in Europe and Eastern North America. Quarterly J. Royal Meteorol. Soc. 146, 1636–1650.
De Vries, A., et al., 2013. Extreme precipitation events in the Middle East: dynamics of the active Red Sea Trough. J. Geophys. Res. Atmos. 118 (13), 7087–7108.
Dinku, T., et al., 2018. Validation of the CHIRPS satellite rainfall estimates over eastern Africa. Q. J. R. Meteorol. Soc. 144, 292–312.
El Fandy, M., 1948. The effect of the Sudan monsoon low on the development of thundery conditions in Egypt, Palestine and Syria. Q. J. R. Meteorol. Soc. 74, 31–38.
Faranda, D., Messori, G., Vannistem, S., 2019. Attractor dimension of time-averaged climate observables: insights from a low-order ocean-atmosphere model. Tellus 71, 1554413.
Faranda, D., Messori, G., Yiou, P., 2017. Dynamical proxies of North Atlantic predictability and extremes. Sci. Rep. 7, 41278.
Funk, C., et al., 2015. The climate hazards infrared precipitation with stations—a new environmental record for monitoring extremes. Sci. Data 2, 150066.
Gasch, P., et al., 2017. Revealing the meteorological drivers of the September 2015 severe dust event in the Eastern Mediterranean. Atmos. Chem. Phys. 17, 13573–13604.
Hersbach, H., et al., 2020. The ERA5 global reanalysis. Q. J. R. Meteorol. Soc. 146, 1999–2049.
Hochman, A., et al., 2019. A new dynamical systems perspective on atmospheric predictability: eastern Mediterranean weather regimes as a case study. Sci. Adv. 5 (6), aau0936.
Hochman, A., De Luca, P., Komacek, T., 2022a. Greater climate sensitivity and variability on TRAPPIST-1e than Earth. Astrophys. J. 938 (2), 114.
Hochman, A., Harpaz, T., Saaroni, H., Alpert, P., 2018. Synoptic classification in 21st century CMIP5 predictions over the Eastern Mediterranean with focus on cyclones. Int. J. Climatol. 38, 1476–1483.
Hochman, A., et al., 2022b. Extreme weather and societal impacts in the eastern Mediterranean. Earth Syst. Dynam. 13, 749–777.
Hochman, A., et al., 2021a. Do Atlantic-European weather regimes physically exist? Geophys. Res. Lett. 48 e2021GL095574.
Hochman, A., Rostkier-Edelstein, D., Kunin, P., Pinto, J., 2021b. Changes in the characteristics of 'wet' and 'dry' Red Sea Trough over the eastern mediterranean in CMIP5 climate projections. Theor. Appl. Climatol. 143, 781–794.
Hochman, A., et al., 2021c. A new view of heat wave dynamics and predictability over the eastern Mediterranean. Earth Syst. Dynam. 12, 133–149.
Hochman, A., et al., 2022c. Dynamics and predictability of cold spells over the Eastern Mediterranean. Clim. Dynam. 58, 2047–2064.
Khodayar, S., et al., 2022. What causes a heavy precipitation period to become extreme? The exceptional October of 2018 in the Western Mediterranean. Weather Clim. Extrem. 38, 100493.
Kidd, C., Levizzani, V., 2011. Status of satellite precipitation retrievals. Hydrol. Earth Syst. Sci. 15, 1109–1116.
Krichak, S., Alpert, P., Krishnamurti, T., 1997. Interaction of topography and atmospheric flow – a possible generator of the Red Sea Trough? Meteorol. Atmos. Phys. 63, 149–158.
Krichak, S., Breitgand, J., Feldstein, S., 2012. A conceptual model for the identification of Active Red Sea Trough synoptic events over the south-eastern Mediterranean. J. Appl. Meteorol. Climatol. 51, 962–971.
Lorenz, E., 1963. Deterministic nonperiodic flow. J. Atmos. Sci. 20 (2), 130–141.
Lucarini, V., et al., 2016. Extremes and recurrence in dynamical systems. In: Extreme Value Theory for Selected Dynamical Systems. Wiley, Hoboken, NJ.
Lucarini, V., Faranda, D., Wouters, J., 2012. Universal behavior of extreme value statistics for selected observables of dynamical systems. J. Stat. Phys. 147, 63–73.
Ludwig, P., Hochman, A., 2022. Last glacial maximum hydro-climate and cyclone characteristics in the Levant: a regional modelling perspective. Environ. Res. Lett. 17, 014053.
Marra, F., Levizzani, V., Cattani, E., 2022. Changes in extreme daily precipitation over Africa: insights from a non-asymptotic statistical approach. J. Hydrol. X 16, 100130.
Messori, G., Caballero, R., Faranda, D., 2017. A dynamical systems approach to studying midlatitude weather extremes. Geophys. Res. Lett. 44, 3346–3354.
Palmer, T., 2000. Predicting uncertainty in forecasts of weather and climate. Rep. Prog. Phys. 63 (2), 71.
Pons, F., Messori, G., Alvarez-Castro, M., Faranda, D., 2020. Sampling hyperspheres via extreme value theory: implications for measuring attractor dimensions. J. Stat. Phys. 179, 1698–1717.
Raveh-Rubin, S., Wernli, H., 2016. Large-scale wind and precipitation extremes in the Mediterranean: dynamical aspects of five selected cyclone events. Q. J. R. Meteorol. Soc. 142, 3097–3114.
Rodrigues, D., et al., 2018. Dynamical properties of the North Atlantic atmospheric circulation in the past 150 years in CMIP5 models and the 20CRv2c reanalysis. J. Clim. 31 (15), 6097–6111.
Saaroni, H., Harpaz, T., Alpert, P., Ziv, B., 2019. Automatic identification and classification of the northern part of the Red Sea Trough and its application to climatological analysis. Int. J. Climatol. 40 (7), 3607–3622.
Satgé, F., et al., 2020. Evaluation of 23 gridded precipitation datasets across West Africa. J. Hydrol. 581, 124412.
Sodemann, H., Schwierz, C., Wernli, H., 2008. Interannual variability of Greenland winter precipitation sources: Lagrangian moisture diagnostic and North Atlantic Oscillation influence. J. Geophys. Res. 13 (D3), D03107.
Sprenger, M., Wernli, H., 2015. The LAGRANTO Lagrangian Analysis Tool – Version 2.0, vol. 8. Geoscientific Model Development, pp. 2569–2586.
Süveges, M., 2007. Likelihood estimation of the extremal index. Extremes 10, 41–55.
Tsvieli, Y., Zangvil, A., 2005. Synoptic climatological analysis of 'wet' and 'dry' Red Sea Troughs over Israel. Int. J. Climatol. 25, 1997–2015.
Wedler, M., Pinto, J., Hochman, A., 2023. More frequent, persistent, and deadly heat waves in the 21st century over the Eastern Mediterranean. Sci.Total Environ. 870, 161883.
Wernli, H., Davies, H., 1997. A Lagrangian-based analysis of extratropical cyclones. I: the method and some applications. Quartely J. Royal Meteorol. Soc. 123 (538), 467–489.
Ziv, B., et al., 2022a. Formation of cyclones over the east mediterranean within red-Sea Troughs. Int. J. Climatol. 42 (1), 577–596.
Ziv, B., et al., 2022b. Identification and classification of the wet Red Sea Trough over Israel. Int. J. Climatol. 1–21.